Available online at www.sciencedirect.com
SCIENCE DIRECT®
Journal of Chromatography A, 1029 (2004) 193–203
JOURNAL OF CHROMATOGRAPHY A
www.elsevier.com/locate/chroma

Novel flame photometric detector for gas chromatography based on counter-current gas flows

Kevin B. Thurbide [a,*], Brad W. Cooke [a], Walter A. Aue [b]

[a] *Department of Chemistry, University of Calgary, 2500 University Drive N.W., Calgary, Alta., T2N 1N4 Canada*
[b] *Department of Chemistry, Dalhousie University, Halifax, NS, B3H 4J3 Canada*

Received 30 September 2003; received in revised form 10 December 2003; accepted 10 December 2003

Abstract

A novel analytical device has been developed for gas chromatography. It is based on optical emission from a counter-current (i.e. counter-flowing) air or oxygen flame, which burns in an opposing stream of hydrogen and column effluent. The flame is typically positioned "upside down" on the upper (air) jet, which faces the lower (hydrogen + effluent) jet. It can also be positioned on the lower jet, be connected to both jets, or be suspended in the gap between them. Excellent stability can be obtained in any of these modes. Overall, this new "counter-current flame photometric detector" (ccFPD) responds to analytes in the manner of a conventional flame photometric detector (FPD); however, it can be operated over a much wider range of gas flows. For instance, the same physical ccFPD burner easily supports stable flames of air flows between 5 and 200 ml/min and corresponding hydrogen flows between 5 and 10,000 ml/min. Visual observation of the counter-current flame, in the presence of sulfur and phosphorus as test analytes, reveals intense, steady luminescence under a wide variety of conditions. Additionally, and in contrast to the commercial FPD, flame conductivity signals can be obtained that are similar in quality to those produced by a conventional flame ionization detector (FID). Thus the ccFPD is a flexible, easily optimized photometric detector. The exceptional flow stability of the ccFPD was used to explore the earlier reported phenomenon of strong signal/noise (S/N) ratios, which had been obtained for hetero-elements of the iron group from a conventional FPD with a small, stoichiometric flame. Results using the ccFPD, which also exhibits this unusual response, indicate that these high S/N ratios are only partly due to the predictable decrease in flame noise with decreasing flame size. Contrary to expectations, the absolute analyte signal often increases as the flame size decreases to the point of extinction. The signal intensity and the magnitude of the observed changes depend to some degree on the flame composition (H_2/O_2 ratio).

Keywords: Flame photometric detection; Detection, GC; Counter-current flame; Instrumentation; Organophosphorus compounds; Organosulfur compounds; Metals

1. Introduction

The flame photometric detector (FPD) has been one of the most widely used detectors in gas chromatography (GC) for over three decades. This is largely due to its sensitive and selective response for compounds containing sulfur, phosphorus, tin, and several other elements [1–9]. During the course of the FPD's extensive use in such areas as pesticide residues, petroleum chemistry, and air pollution, several other devices have been developed that incorporate similar operating principles and hence impart FPD-like responses. Examples include the dual-flame FPD [10], the pulsed-flame FPD [11–13], and the reactive-flow detector [14].

In recent years a study from our (Dalhousie) group demonstrated that an FPD using a small, stoichiometric flame could produce unexpectedly sensitive signal/noise (S/N) responses for iron-group metals [15]. It was found that its iron, ruthenium, and osmium emissions consisted of very similar spectral continua. This contrasts with the typical atomic lines and metal-oxide molecular band systems that some of these metals, e.g. iron, are known to generate in the larger flame of a conventional FPD [16], in the pulsed-flame FPD [12], and of course in the still far hotter flames or plasmas of atomic spectroscopy. Furthermore, the S/N response increased steadily as the flame was made progressively smaller. Ultimately, the small, stoichiometric flame bordered on extinction when some of the

* Corresponding author. Tel.: +1-403-220-5370; fax: +1-403-289-9488.
E-mail address: thurbide@ucalgary.ca (K.B. Thurbide).

0021-9673/$ – see front matter © 2004 Elsevier B.V. All rights reserved.
doi:10.1016/j.chroma.2003.12.020

lowest MDLs (minimum detectable limits) were recorded. These compared favorably with the best values reported for atomic emission detection, making this FPD method a useful alternative for the GC analysis of volatile organometallic compounds of these metals [15] (or of their ions after appropriate derivitization [17]). However, flame extinction limited the study of this excitation source at still lower gas flows, and hence prevented a better spectrochemical understanding of the underlying phenomena.

For instance, the fact that the analytical emissions of these elements are spectrally different in flames of different size and composition is easily rationalized. However, it is quite remarkable that the S/N ratios increase so strongly as the size and energy of the flame is lowered. Since much lower (as well as much higher) gas flow conditions were not accessible on the then-used system, the response characteristics of a still weaker flame, and how it would compare to a much larger flame of the same composition, had to remain unknown. Such information about signal and noise over a wide range of flame conditions could, however, have been quite helpful in understanding the mechanism of the strong emission. But in order to conduct a study of this nature, a more stable flame system was needed.

In its most conventional design, the FPD is based on photometric emissions emanating from a fuel-rich hydrogen–air flame receiving GC effluent. The flame burns on a set of concentric tubes that deliver the reagent gases. This is a common burner design [18]. Similar burners/combustion modes (e.g. premixed flames, etc.) produce reliable responses in a multitude of other flame-based GC detectors [19]. As well, a variety of interesting slot or multi-capillary type burners have served to sustain larger flames for analytical use, for spectroscopic excitation [20–22], or for monitoring gas-phase reactions [23].

Indeed, combustion research has often been facilitated by the advent of novel, unconventional burners, which are then used to study such topics as the ignition, stability, flow profiles, and burning velocity of flames [24]. Counter-current flames are a good example of this. In this respect, “current” refers to the flowing current of flame gases, and is sometimes also referred to as a “counter-flowing” flame. In these systems, fuel and oxidant are introduced as opposing gas streams from burners directly opposite (usually above and below) one another [25,26]. This unique burner arrangement is frequently used to study combustion flow profiles and flame structure during ignition. Yet despite its potential analytical interest, we are not aware of any prior study where such a system has been incorporated into a GC detector.

Recently, during a study of various GC burner designs, we began working with counter-current flames. Their remarkable stability and emission characteristics strongly suggested future analytical usage, especially where either very small or very large flames had to be accommodated. For instance, subsequent to this study, our (Calgary) group found that small counter-current flames could be potentially helpful for portable, miniaturized, low-flow analytical devices [27,28]. This format also differs from other micro-analyzers employing more conventional flames [29,30]. On the other hand, larger counter-current flames may prove to be beneficial to supercritical fluid chromatography, where large volumes of rapidly expanding carrier must enter the detector. Of particular interest, however, was the counter-current flame’s potential to overcome the stability limitations encountered earlier with the small, stoichiometric FPD flame [15].

In this study, we construct a counter-current flame device and operate it as a photometric GC detector, in order to examine the extent to which useful analytical responses can be derived from such a system. Additionally, the response characteristics of this “counter-current FPD” (ccFPD) are evaluated over a wide range of conditions and for a number of photometrically active elements. Some discussion of flame chemistry and structure, as they relate to analyte emission, are also presented.

2. Experimental

A schematic diagram of the ccFPD is shown in Fig. 1. The device rested on the base of a commercial flame ionization detector (FID) atop a GC (a Tracor model 550 in earlier, a Shimadzu model GC-8a in later studies). A new housing was constructed from a 3 in. × 4 in. aluminium block machined to

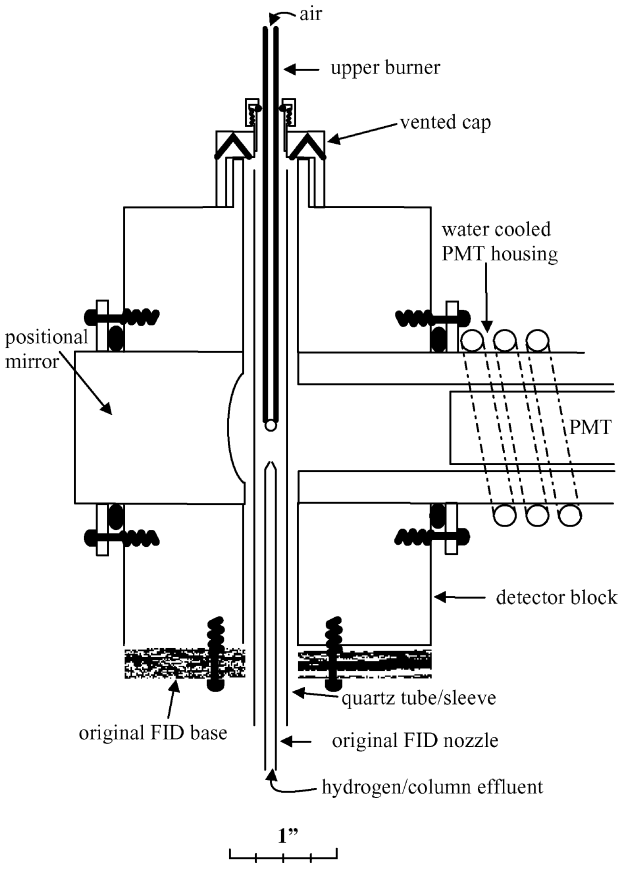

Fig. 1. Schematic view of the ccFPD.

fit the GC detector base (1 in. = 2.54 cm). A 2 cm i.d. hole was drilled vertically through the housing. It accommodated a 10 mm i.d. quartz tube, which surrounded the original detector burner and extended through its full height inside.

The top of the housing was machined to fit a cap. This cap contained holes that allowed flame exhaust to leave, but not light to enter. Through the center of the cap was threaded a 1/4 in. Swagelok stainless steel tube stub that guided a 6 mm o.d. × 1.8 mm i.d. stainless steel burner tube downward, to any desired height opposite the original FID burner nozzle. Horizontally through the center of the block, a 1.5 in. i.d. hole was drilled. Into one end of this hole, a movable aluminium cylinder with a polished concave mirror was inserted and held in place by an O-ring. From the other end, a water-cooled photomultiplier tube (PMT; R-374 or R-1104 with wavelength range 185–850 nm; Hamamatsu, Bridgewater, NJ, USA) was pushed in through an O-ring. Its photocathode was situated directly opposite the mirror for efficient light collection.

Typically but not exclusively, hydrogen and column effluent were introduced into the quartz enclosure through the original FID nozzle (forming the 'lower burner') and air was delivered from the top through the 'upper burner'. A borosilicate column, 2 m × 1.8 mm i.d., packed with 10% Apiezon L on Chromosorb W (45–60 mesh), was used to perform separations on the Tracor instrument with a typical nitrogen flow of 12 ml/min through the column. Separations on the Shimadzu instrument were performed on an EC-5 [(5% phenyl)-95% methylpolysiloxane] megabore column (30 m × 0.53 mm i.d.; 1.00 μm thickness; Alltech, Deerfield, IL, USA), using 5 ml/min of helium as carrier gas. Chemicals for standard solutions were used as received from Aldrich, and gases were obtained from Praxair. Spectra were acquired using a 1/4 m Jarrell-Ash monochromator (1180 lines/mm grating, 3 nm/mm bandpass), or an Oriel model 77250 1/8 m monochromator (No. 77298 grating; 1200 lines/mm, 6 nm/mm bandpass). Other variations, as well as the optimized gas flow settings, are described later.

3. Results and discussion

3.1. General operating parameters

The unique arrangement of fuel and oxidant gases entering in opposite, i.e. "counter-current" directions allows great flexibility in situating and operating the flame at various positions and conditions within the detector. We have examined numerous parameters and found that the ccFPD system is able to produce stable flames in a variety of easily controlled operating modes. Most notably, this apparatus can support flames situated on the lower burner, flames on the upper burner, flames disconnected from but stably suspended between the two burners, or even flames connected to and spanning the full distance from the upper to the lower burner. These flames can assume oval, flat, bell-shaped and many other forms, in very small and also in very large sizes.

The common and consistent observation made in practically all of these cases is that the flame, at appropriately chosen conditions, remains stable and does not flicker or extinguish, even when a 10-μl solvent injection is made, or when the burners are placed off-axis to one another. Of further interest is that, depending on the ccFPD burner arrangement, the system can produce stable flames by using gas flows ranging from only a few milliliters all the way up to several liters per minute. As one might expect, the resulting flames vary greatly in size, shape and temperature. For example, the use of 30 ml/min each of hydrogen and air results in a roughly spherical counter-current flame of about 3 mm diameter, which registers about 200 °C on a thermocouple dipped into the lower, hydrogen-rich region where analytes such as sulfur emit (although, nearer to the upper burner, the outer and inner cone regions measure about 500 and 900 °C, respectively). In contrast, when using much larger flows of 200 ml/min of air and 10 l/min of hydrogen, the resulting flame is about 10 mm in diameter and measures 1200 °C at its center, due to the inner cone extending throughout much of the visible flame volume. Since both air or oxygen counter-current flames can be readily supported in the opposing stream of hydrogen, the ccFPD device has the potential of providing a variety of unique flame conditions/compositions within the region spanning the two burner jets.

A number of burner arrangements were initially tested in simple glass housings, in order to observe the process by naked eye. Typically, the two opposing burner jets, of inside diameters between 0.5 and 10 mm, were examined at varying distances between 1 and 30 mm from one another. While all trials supported flames over a wide range of gas flows, the most stable counter-current flames were obtained when the upper air tube was situated inside the lower quartz tube, which was of slightly larger diameter and carried the counter-flowing stream of hydrogen and column effluent. In order to preserve chromatographic resolution, the original narrow-bore FID nozzle was later incorporated into the quartz tube, which formed a sleeve around the upper air burner (see Fig. 1). In this way, the upper air tube was fully contained within the lower hydrogen/effluent tube. This is an unconventional set-up compared to arrangements typically used in counter-current combustion studies [25,26]. In such a 'tube inside a tube' mode, the most stable and versatile counter-current flames were produced on a stainless steel upper burner (2 mm i.d. tubing × 2 mm wall thickness) situated inside a quartz sleeve (10 mm i.d. tubing × 1 mm wall thickness). This arrangement was used in subsequent experiments and is represented in Fig. 1, which shows the air burner at a typical separation gap of about 10 mm from the original FID nozzle. Also indicated in Fig. 1 is the characteristic flame burning upside down (or, so to speak, 'hanging from') the upper air burner into the counter-flowing stream

of hydrogen plus column effluent emerging from the FID jet below.

3.2. General characteristics

3.2.1. Background and noise of the pure flame

In general, and similar to a conventional FPD, the ccFPD's baseline appears to be comprised of fundamental, i.e. "white" (random) noise, which is correlated to the square root of the number of photoelectrons generated by the PMT. This can be illustrated by using the rms $= (Ieg/t)^{1/2}$ relationship, where rms is the root-mean-square (Gaussian standard deviation) of the baseline fluctuations, I the baseline current in A, e the charge of the electron (1.6×10^{-19} A s), g the photomultiplier gain for the voltage used, and t is the integration time of the measurement (i.e. the effective time constant of the acquisition system) [31]. Under typical ccFPD conditions employing a PMT gain of 3×10^4 (at 700 V as specified by the manufacturer) and a system time constant of 1 s, the resulting baseline current of 457 pA is found to generate 1.7 pA of noise, which compares well with the calculated value of 1.5 pA. This implies that there is very little "flicker" noise present in the ccFPD baseline generated by the background flame emission. While we have not carried out extensive studies of ccFPD noise characteristics, it is interesting to note that these findings do agree with the visual observation of a smooth, stable flame emission.

For a hydrogen–air flame as shown in the ccFPD arrangement of Fig. 1, a considerable range of gas flows are available that provide stable flames. We investigated flows from 5 to 10,000 ml/min of hydrogen and 5–200 ml/min of air. For a given set of conditions, the background level, and hence its noise, increases with increasing air and decreasing hydrogen flow. Thus, the lowest background emission is generally obtained at relatively high hydrogen and low air flow settings.

This behavior is as expected and its origin can be confirmed visually. If the air flow is decreased, the flame front that extends from the upper air burner becomes smaller and smaller, until ultimately parts of it appear to retreat into the stainless steel tube (burner jet). Thus, for lower air flows, the tube shields some of the brightest parts of the flame from view of the PMT, thereby causing the background to decrease (in addition to the general decrease caused by the reduction in temperature). Comparable results can be obtained in the ccFPD by using paint-blackened quartz tubing as the upper burner; however, stainless steel is better suited to the task. This shielding effect, here exerted upside-down, is reminiscent of early commercial FPD models. These included a steel cylinder that surrounded the lower parts of the flame like a cup and could be raised or lowered for maximizing the S/N ratio.

Generally, increasing the hydrogen flow decreases the flame's background emission intensity and extinguishes occasional glowing from the burner tip. This is easily rationalized by considering the extremely high thermal conductivity of hydrogen and, consequently, the much lower temperatures of an air flame front immersed in a hydrogen counter-flow.

3.2.2. Ionization responses of the ccFPD

The question of whether the counter-current flame would produce analytically useful levels of electrical conductivity was obvious, interesting, and easily answered. The system was run with (optimized) flow rates of 20 ml/min hydrogen and 130 ml/min air, and with the existing electric leads from the original GC–FID unit. The FID polarizer was positioned at the upper air burner, and the FID collector at the lower hydrogen/effluent jet. Under these conditions, the counter-current flame proved highly sensitive to the test compounds dodecane and naphthalene. For example, dodecane yielded an MDL of 10 pg/s of carbon, with a sensitivity of 10 mC/g of carbon. These figures-of-merit agree well with the FID's literature specifications [19,32].

The extraordinary stability of the counter-current flame allows facile switching from low to high flow rates, and from hydrogen-rich to air-rich environments. Hence, it is easy to alternate between conditions optimized for either optical or electrical response. That this is significant can be appreciated from the fact that conventional FPD constructions often include electrical sensors. These are obviously designed to accommodate analytical customers. However, the response of such merely added conductivity sensors is noisy and far below that of an FID proper. In order to obtain optimum photometric or optimum ionization responses from these units, the operator is often required not just to change flame conditions but to reverse detector gas inputs and/or burners. Such rearrangements are not necessary for the ccFPD, which may also not demand large changes in flame conditions when being switched from one type of response to the other.

For instance, it was found that the counter-current flame conditions for producing optimal ionization signals from reduced carbon were not all that different from those providing optimal chemiluminescence signals from sulfur, phosphorus, and other standard analytes tested later in this study. It is therefore possible to obtain simultaneous electrical and optical signals from the ccFPD, with a minimum of degraded performance in either. This opens the possibility of two-dimensional response with the desired minimum of correlation between the two detector response characteristics. Such two dimensional response has been investigated previously in a variety of detector formats [13,33,34]. While the counter-current flame approach may also prove useful to other established gas chromatographic sensors, such as the well-known nitrogen–phosphorus detector (NPD) [1–3], no such experiments were initiated in the current study.

3.3. Photometric response of sulfur and phosphorus

Since its introduction, the conventional FPD has most often been used to analyze compounds containing sulfur and

phosphorus, and a large amount of literature is available on the results. It is therefore incumbent on a study like this to examine how well the ccFPD can emulate the responses of the conventional FPD to these two benchmark analytes.

With tris(pentafluorophenyl)phosphine as the test compound, the optimal flame gas flows for phosphorus in the ccFPD are found to be 95 ml/min of hydrogen and 141 ml/min of air; with ethyl sulfide as the standard analyte, optimal ccFPD response for sulfur is obtained at 40 ml/min of hydrogen and 91 ml/min of air. Incidentally, these optimal-flow settings are found to decrease somewhat when a tube of slightly larger diameter is used for the upper air burner. However, this decreases flame stability and does not improve response: it has therefore not been investigated further. As well, the addition of up to 10 ml/min of nitrogen or argon to the hydrogen flow increases the optimal response in some cases. While similar increases have been noted in the literature for the conventional FPD, the effect is likewise not well reproduced in the ccFPD and only yields an improvement factor of less than five.

Of greater interest is that the optimal ccFPD flame gas flows for both sulfur and phosphorus, while still hydrogen-rich, are close to stoichiometric values (H_2/O_2 ratios between about 2 and 3). This is in contrast to the optimal gas flows in a conventional FPD, which are usually much richer in fuel (H_2/O_2 ratios between about 4 and 10) [18]. This feature of the ccFPD may prove quite useful. As alluded to earlier, the difference between the optimum flowrates for the ionization response toward carbon on one hand, and the photometric response toward sulfur, phosphorus and other elements on the other, is much smaller in the ccFPD than in the conventional FPD. This makes it fairly easy to establish a compromise flowrate that will yield analytically acceptable optical and electrical responses at a single set of conditions and for a greater variety of hetero-atoms. The cause of this pronounced difference in optimum gas composition between the two detector types is likely related to the structure of the flame.

Fig. 2 depicts the difference between the typical flame of a conventional FPD (Fig. 2a) and that of the ccFPD (Fig. 2b). As schematically illustrated here, the conventional FPD often produces flame profiles with oblong or pointed inner and outer diffusion cones. In comparison, the ccFPD creates a flame that is much more compact and spherical. Perhaps more importantly, in the most common form of the conventional FPD, analyte enters the flame concentrically about the axial air burner. Under these conditions, at least some of the analyte is first exposed to the relatively high-temperature, oxidizing environment of the flame's inner cone, and it is likely that a considerable amount of the eluting sulfur and phosphorus is first converted to oxygenated species. Such conversion certainly takes place in the original Brody-Chaney FPD design, which adds analyte to the flame via the air stream [35]. Pre-oxidation is also deliberately supported in some successful dual-flame FPD designs that initially burn the analyte in an oxygen-rich flame

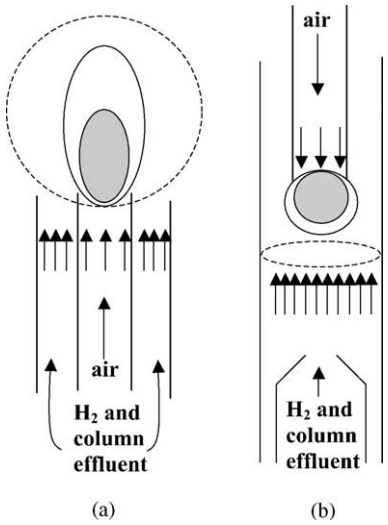

Fig. 2. Illustration of gas flow dynamics in (a) the conventional FPD and (b) the ccFPD. The superimposed dashed lines depict the region where sulfur emission is typically observed.

before passing it on to a second, hydrogen-rich flame for emission monitoring [36].

In contrast, in the ccFPD the analyte is first subjected to the relatively cool and hydrogen-rich environment prevailing below the counter-current flame. Under these conditions, any reduced precursors to analyte excitation may be formed directly, without oxygenated intermediates [17]. This is consistent with our visual observation of the two detectors. For instance, sulfur emission in a conventional FPD typically occurs in a region encompassing the entire flame volume and especially the peripheral area, as indicated by the dashed line in Fig. 2a. In contrast, sulfur emission in the optimized ccFPD appears as a centered "disc", well ahead ("ahead" in terms of analyte flow) of the counter-current flame situated on the upper burner (Fig. 2b). Clearly, this process is facilitated by the fast diffusion and relatively slow recombination of hydrogen atoms. Under comparable conditions, it has been demonstrated that considerable degradation of hetero-atomic compounds (as well as concomitant analyte emission) can occur in hydrogen-rich environments outside the visible hydrogen-air flame region [23,37]. These findings indicate that precursor species to chemiluminescent excitation are formed well before the analyte reaches the basic flame.

The responses to different amounts of phosphorus- and sulfur-containing analytes were measured with gas flows corresponding to S/N maxima. The results are given in Fig. 3. As shown there, the response to phosphorus remained linear for about four-orders of magnitude, down to a minimum detectable flow of 1×10^{-12} gP/s at an extrapolated S/N ratio of two (noise was measured as the peak-to-peak fluctuations of the baseline). Similarly, the response to sulfur yielded the familiar non-linear slope and a minimum detectable flow of 2×10^{-11} gS/s. Also included in Fig. 3 is the response toward carbon, which

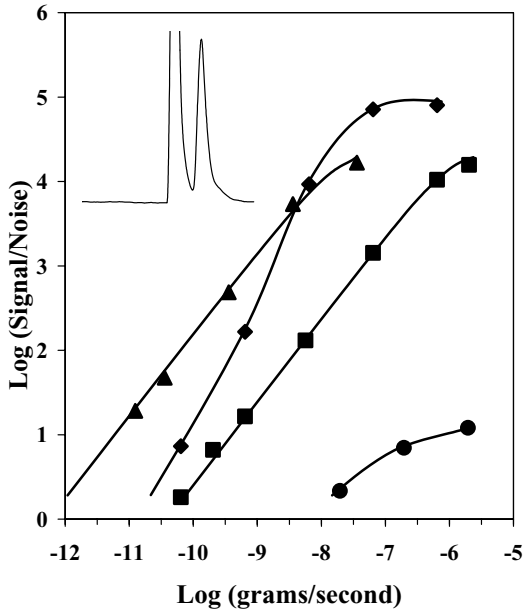

Fig. 3. Calibration curve in the ccFPD for phosphorus (▲) as tris(pentafluorophenyl) phosphine, sulfur as tetrahydrothiophene (◆), and carbon as benzene(●) in the filterless, non-dispersive mode, and sulfur as tetrahydrothiophene (■) monitored through a 590 nm long pass filter. Conditions are listed in the text. Inset: a GC-ccFPD chromatogram showing a 1 μg injection of trimethyl phosphite eluting just after the solvent peak.

was found to be approximately the same under either optimum-sulfur or optimum-phosphorus conditions. Carbon response was non-linear with a slope of less than one, over only one-order of magnitude, down to a minimum detectable flow of 2×10^{-8} gC/s. This translates into a phosphorus-over-carbon selectivity (i.e. mol P/mol C for peaks of equal height) of about four-orders of magnitude, and a similar sulfur-over-carbon selectivity of about three-orders of magnitude (as measured at lower range). These values agree very well with those of the conventional FPD [18], indicating that the two detector types produce similar responses to sulfur and phosphorus. Spectra of migrating peaks confirm that, as in the conventional FPD, the blue sulfur emission of the ccFPD stems from S_2^*, while its green phosphorus emission originates from HPO^*. Accordingly, by adding a 394 nm or a 520 nm interference filter to the photometric channel, the respective ccFPD responses towards sulfur and phosphorus could be monitored with increased selectivity.

3.3.1. Linear sulfur response

Given the similarity of the ccFPD's behavior to that of a conventional FPD, it seemed reasonable to investigate its response toward sulfur above 600 nm. In this region, the excited sulfur species HSO^* provides the conventional FPD, the pulsed-flame FPD, and the reactive flow detector with linear sulfur response, albeit at lower sensitivity than the quadratic S_2^* [11,14,38]. This occurs despite the fact that the red HSO^* chemiluminescence is not visually observable and can only be monitored by suppressing the blue S_2^* bands through the use of a long-pass and/or interference filter [14,38].

Initial attempts to observe HSO^* in the ccFPD made use of the same 590 nm long-pass filter that enabled linear sulfur response to be monitored in the conventional FPD. However, in the ccFPD this filter resulted in little change to the slope of the calibration curve, indicating that S_2^* still remained the dominant observable emission. Subsequent attempts to optimize the lower hydrogen and upper air flows, or to monitor different regions of the counter-current flame also failed to yield any substantial evidence of the HSO^* bands.

The mechanism of HSO^* formation in the FPD has not been elucidated. However, if a precursor such as SO is required to react with a hydrogen radical in order to form the excited species, then an oxygen-richer environment should facilitate the formation of HSO^*. Such an environment would be chemically similar to the region surrounding the inner air cone of the conventional FPD flame, where HSO^* is readily produced.

In order to test this hypothesis, we added air to the lower hydrogen burner such that the counter-current flame remained situated on the upper air tube, but was now burning in an opposing stream of hydrogen and air. With optimized flows of 91 ml/min air through the upper tube, and 210 ml/min hydrogen plus 90 ml/min air through the lower tube, this approach proved successful. As Fig. 3 demonstrates, the addition of premix air to the hydrogen flow contributes to the formation of HSO^* and results in a linear calibration curve that spans about four-orders of magnitude down to a minimum detectable flow of 7×10^{-11} gS/s. These figures agree well with those found earlier for HSO^* emission in a conventional FPD [38].

As mentioned above, the red HSO^* emission is very difficult to detect visually amidst the prominent blue S_2^* luminescence in a conventional FPD, even if the flame is optimized for HSO^* response. In comparison it is interesting to note that in the ccFPD, with air added to the hydrogen stream and conditions optimized for HSO^*, the red emission is readily seen and much less blue emission appears. This suggests that the ccFPD may be capable of providing additional optimization parameters for elements with more than one emitting species. However, no experiments have yet been carried out on this topic.

3.4. Photometric response of metals in the ccFPD

3.4.1. Flow conditions

The ccFPD's performance for sulfur and phosphorus having thus been established, its response toward several metals was investigated over a wide range of gas flows, some of which had not been available to the earlier stoichiometric FPD flame study [15]. The metals chosen for testing were primarily those that had shown unexpected sensitivity at that time. And, indeed, initial optimization of

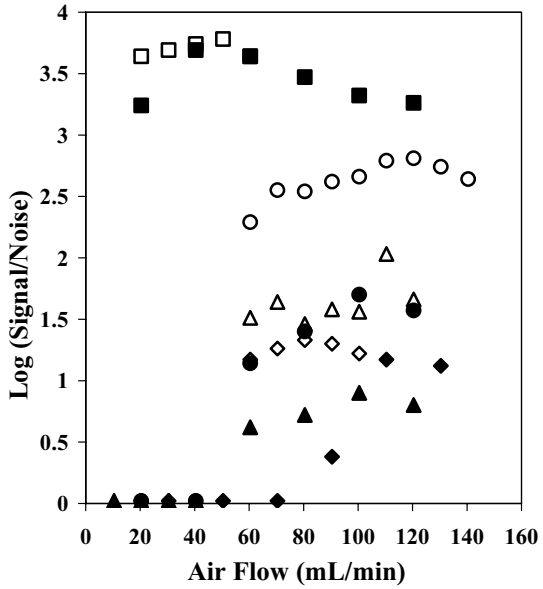

Fig. 4. Response of ferrocene (closed symbols) and ruthenocene (open symbols) in the ccFPD for various air flows at hydrogen flows of 300 (◆), 90 (▲), 20 (●), and 5 (■) ml/min.

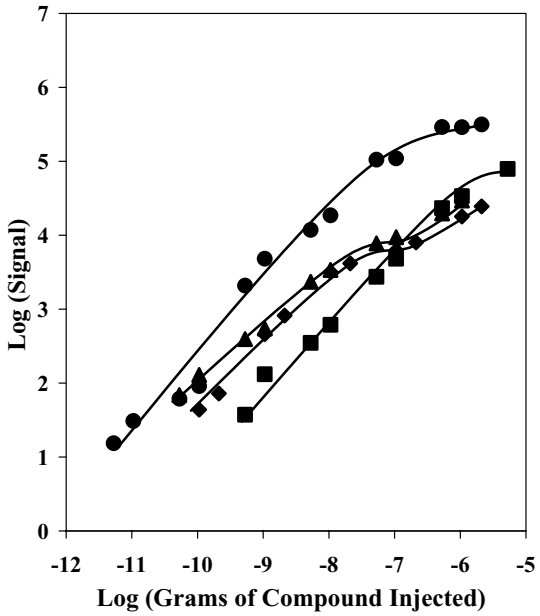

Fig. 5. Calibration curve of ferrocene (▲), ruthenocene (●), tetraethyl lead (■), and MMT (◆) in the ccFPD. Flame gas flows are 5 ml/min of hydrogen and 20 ml/min of air.

the ccFPD responses to iron and ruthenium clearly indicated a dramatic increase in S/N as the flame decreased in size and decreased in hydrogen flow, to the point of becoming stoichiometric or even air-rich.

Fig. 4 displays some of these S/N curves from the optimization procedures for ferrocene and ruthenocene. In the ones shown here, the air flow was varied for several constant settings of hydrogen flow. As can be appreciated from Fig. 4, the S/N range for each of the different sets increases several orders of magnitude as the hydrogen flow decreases from 300 ml/min to 5 ml/min, and as the maxima shift to lower air flow rates. For these iron-group metals, then, the ccFPD provides the best response under conditions that yield a relatively small, slightly air-rich flame. This agrees with the behavior of the small stoichiometric flame employed previously in a conventional FPD [15]. It contrasts, however, with earlier studies that made use of much larger, hydrogen-rich FPD flames [39]. Such a contrast is not surprising, though, since the two studies optimized and monitored different spectral features. For example, iron produces a broad continuum in a small, stoichiometric flame, but emits atomic lines (and minor molecular bands) in a larger, strongly hydrogen-rich flame.

Fig. 5 shows the calibration curves for ferrocene and ruthenocene under S/N-optimized conditions in the ccFPD. Also included in Fig. 5 are compounds of the main-group element lead (as tetraethyl lead) and the non-iron-group element manganese (as MMT, i.e. methylcyclopentadienyl manganese tricarbonyl). Overall, the analytical figures-of-merit compare well with those of the small, stoichiometric FPD flame [15] and confirm that, as anticipated for these metals, the ccFPD offers similar performance.

In this context it is fortuitous that the ccFPD extends the experimental flow conditions considerably beyond those of the conventional FPD. In other words, this represents an opportunity to use the ccFPD's wider flow range to investigate how certain flame parameters such as size and stoichiometry affect metal response. Such information is of interest not only to the problem of the small stoichiometric flame study [15], but also to a wider range of questions, touching even on atomic flame spectroscopy. To wit, from the latter perspective it would seem rather odd that a flame should be more effective the smaller and cooler it became and that, indeed, it should render its best analytical performance just before it expired.

A particular feature of Fig. 5 warranted further exploration. While ruthenium and lead yield linear calibration curves (slope = 1 in a log–log plot) over much of their range, iron and manganese start at a gentler slope that further decreases and then, unexpectedly, increases again. Since there appeared to be no obvious reason for this behavior, further experiments were carried out to characterize the effect of flame composition on the calibration curve.

Fig. 6 does this for ferrocene, using hydrogen flows at or near the optimum value of 5 ml/min, together with an air flow appropriate for the chosen molar gas ratio. The tilde-shaped calibration for iron is again apparent, here for H_2/O_2 ratios of 1 and 1.3. This effect appears to vanish, however, for the purely stoichiometric flame of $H_2/O_2 = 2$. The slope of that calibration curve is 0.75, as it is in the lower portions of the two nearby curves. Whether this 3/4 exponent is accidental or indicates a complex kinetic relationship is at present unknown.

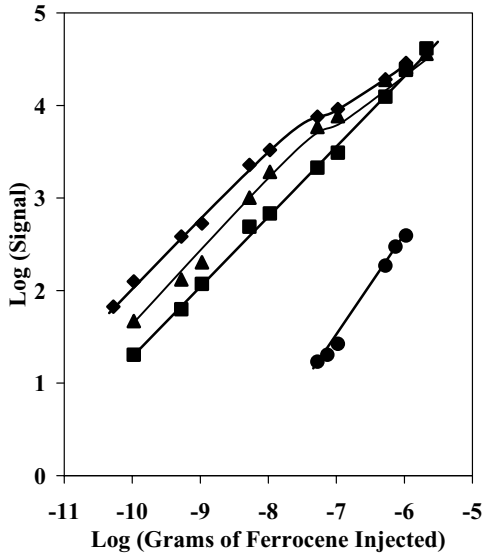

Fig. 6. Calibration curve of ferrocene in the ccFPD using flames of different stoichiometry. The hydrogen and air flows in ml/min (with the hydrogen/oxygen ratio given in brackets) are: 5 and 25 (1) (▲), 5 and 20 (1.3) (◆), 8 and 20 (2) (■), and 24 and 90 (1.3) (●).

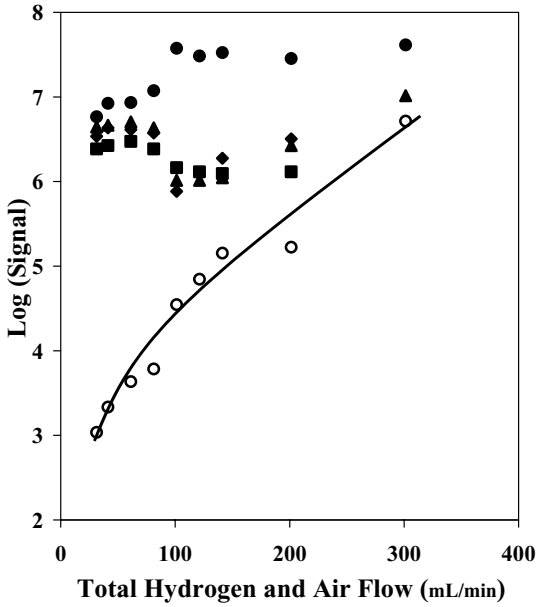

Fig. 7. Response of ferrocene (▲), ruthenocene (●), tetraethyllead (■), MMT (◆), and the corresponding baseline peak to peak noise (○) in the ccFPD for various flows of hydrogen and air that create a counter-current flame of fixed stoichiometry. The hydrogen/oxygen ratio is 1.

As shown in the figure, the iron response decreases within an order of magnitude when the gas supply changes from its optimum hydrogen/oxygen (as air) ratio of 1.3, to 1 (air-rich) or 2 (stoichiometric). However, as expected from the optimization trials, significantly hydrogen-richer settings decrease the response severely. For instance, a hydrogen/oxygen ratio of 4 (hydrogen: 24 ml/min, air: 30 ml/min) provides little or no response to microgram injections of ferrocene (not shown in Fig. 6). Thus, analytically useful response toward iron in the ccFPD is clearly obtained from flames that are leaner in hydrogen. Spectral examination of the iron emission under optimum S/N conditions reveals a continuum situated between about 350–500 nm. While few distinguishing features appear superimposed on this continuum (at an optical bandpath of 6 nm), it does emit in the same region as, and bears a coarse resemblance to, the iron-oxide band systems observed in the conventional FPD [16].

Given that the S/N-optimized ccFPD flame composition for the iron group is found at a hydrogen/oxygen ratio of about 1.3, it is further interesting to investigate how the size of this flame at the same stoichiometry affects response. Fig. 6 therefore includes a larger flame, also of $H_2/O_2 = 1.3$, which uses 24 ml/min of hydrogen and 90 ml/min of air. As seen in the figure, the smaller flame, with a total flow of 25 ml/min, yields a much more sensitive response than the larger flame with a total flow of 114 ml/min. In fact, the analyte amounts required to elicit the same ccFPD response differ by an astonishing 3.5-orders of magnitude between these two flames of equal H_2–O_2 composition. (Note that the two slopes differ slightly and that the cited ratio of response-equivalent analyte amounts therefore depends, though to a minor degree, on the signal level at which the evaluation is made.) The ccFPD experiments thus establish the superior sensitivity of a small, slightly air-rich flame toward iron (as well as toward several other metals) compared to much larger flames of the same composition.

3.4.2. Flame size and composition

Since Fig. 6 uses "signal" rather than "signal/noise" values as the ordinate, it indicates directly that the analyte emission can actually increase while the flame size decreases. The fact that absolute response would increase in this fashion, even at the approach to flame extinction, was entirely unexpected. In this context it is important to distinguish between "signal" and "signal/noise", with their different spectral and analytical connotations, for a ccFPD flame of changing size. A series of experiments, using intensity ordinates and including noise measurements, was therefore designed to investigate the extent and generality of this behavior; its dependence on composition and size of the ccFPD flame; and its potential applicability to other analytes, such as transition and main-group metals.

Figs. 7–9 address these issues, and show the signals of standard analytes containing iron, ruthenium, lead, and manganese from ccFPD flames increasing in size (here indicated by the "total flow" of fuel gases) at constant hydrogen/oxygen ratios. The ratios are 1 (air-rich, Fig. 7); 2 (stoichiometric, Fig. 8); and 4 (hydrogen-rich, Fig. 9). In each case the total flow of hydrogen and air was varied between the extremes of approaching flame extinction and reaching detection limit. It should be noted that, across the three sets of runs, the generated energy of the flame was not exactly proportional to the total flow of its fuel gases.

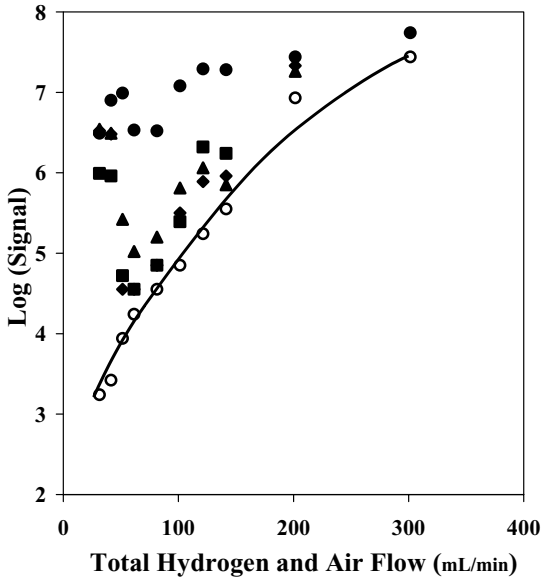

Fig. 8. Same as Fig. 7 except the hydrogen/oxygen ratio is 2.

For instance, at 60 ml total flow (the approximate position of minima in several curves) the flows of H_2O(g) generated were 10, 17.2 and 13.3 ml/min in Figs. 7–9, respectively.

Examination of the curves illustrates that, as the total gas flow increased from about 25–300 ml/min, the corresponding noise increased by roughly two (hydrogen-rich) to four (air-rich) orders of magnitude. (Note that the ordinates of Figs. 5–9 use the same arbitrary units, i.e. peak height times attenuation, and that data can therefore be freely compared among graphs.)

The increase in noise leads to a commensurate decrease in the signal-to-noise ratio for each test analyte. Spectral examination of the flames indicates that the sole monitored background emission was that of OH* (maximum at ca. 306 nm). This spectral feature increased greatly as the total flame gas flow increased. It correlates with the observed increase in the noise (see above) and originates in the inner cone of the flame.

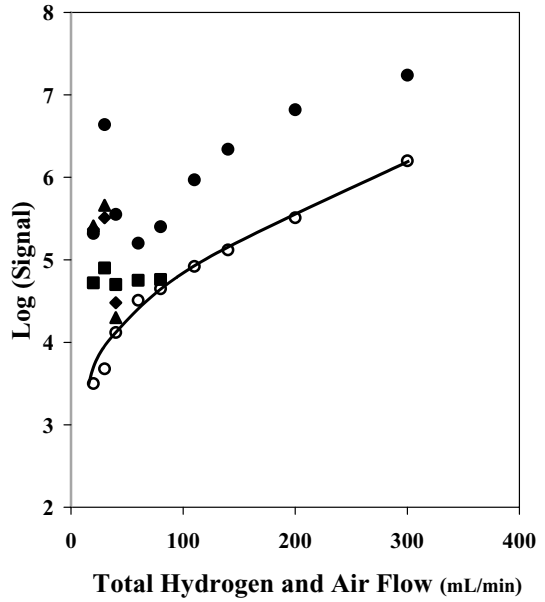

Fig. 9. Same as Fig. 7 except the hydrogen/oxygen ratio is 4.

What is most striking about Figs. 7–9 is the variation in analyte signal as the total flow decreases. For the stoichiometric and hydrogen-rich flames (Figs. 8 and 9), the signal weakens as the flame size decreases, but only until the total flow reaches about 60 ml/min. With further decreases in flame size the signal begins to strengthen again, in some cases quite dramatically. In the air-rich flame (Fig. 7), a similar behavior is observed for Fe, Pb and Mn, although this now occurs at ca. 100 ml/min of total flow. The Ru curve differs in shape from those of the three other elements, but still shows a shift at the same flow rate.

It is not clear why minima should be observed or why signal strength should increase at lower flows. The fact that a similar pattern of behavior is observed for such disparate elements as Fe, Pb, Mn and Ru argues for an effect of the flame rather than of a particular analyte. Yet, a change in emitting species could not be ruled out by experiment, since the S/N ratio is too small at high flowrates for adequate spectral analysis.

The noise curves are smooth and correspond to what one would expect for a flame that changes evenly in size, energy and temperature. In contrast, the analyte signal curves show minima. In fact, one could interpret the analyte signal as the superimposition of two curves, one dominating at low, the other one at high flowrates (and temperatures). If this were the case, it would be tempting to assign the former to chemical, the latter to thermal excitation.

However, the counter-current flame is very small and the analyte signal, besides being found in different flame regions, is very weak on an absolute basis (e.g. compared to typical atomic-spectroscopy flames). Given this, it would be quite difficult to establish and define the extent of thermal emission. We therefore mention this scenario simply as a point for future discussion.

Also worth discussing is the question whether the extremely small ccFPD flames are not too small to produce FPD-like behavior. For instance, calibration linearity could be clearly affected if the molar ratio of relevant flame gas flow to analyte flow became too small.

As is well known, several orders of linear response are commonly obtained for many elements in the larger flame of the conventional FPD. This results from the fact that the bi- or ter-molecular reactions, which excite the emitting analyte species, appear here in pseudo-first-order. This occurs since the large reservoir of energy-carrying flame radicals dwarfs the minute amounts of analyte. However, a basic calculation of the molar ratio of flame gases and analyte flow indicates that this is also likely the case for the very small flame of the ccFPD. We shall select ferrocene and the optimized conditions of Fig. 5 as an example for the following demonstration.

Under optimized conditions, 5 ml/min of hydrogen and 4 ml/min of oxygen (as 20 ml/min air) support a ccFPD flame that is close to extinction. Even for a ferrocene peak of 10^{-6} g (with a half-width of about 10 s) the flame gas flow exceeds the analyte flow, very approximately, by four-orders of magnitude on a molar basis. For the smallest injected amounts of ferrocene, this difference increases a further few orders. Compare this to the difference (in flow) between the smallest flames discussed in this study and the conventional flames of the FPD [18]: this difference is merely one-order of magnitude. Based on this evidence it seems unlikely that the non-linearities of the calibration curve could be attributed to an inadequate molar relationship between flame and analyte.

Furthermore, the flame of Fig. 5 consumes 2.5 ml/min of the available oxygen. That leaves 1.5 ml/min for converting the carbon and hydrogen of analyte peaks to carbon dioxide and water. To wit, in the above mentioned case of 1 μg of ferrocene eluting in 10 s, the carbon and hydrogen of the two cyclopentadienyl rings in each molecule would use up 25 oxygen atoms. This amounts to just less than one percent of the available oxygen. Thus, even when including the total combustion of the test compound in the calculation of the molar excess of flame gases, and assuming typical levels of column bleed and carrier contamination, the size of the flame still does not appear to be an issue.

The problem, in this as well as in other cases, is that the precise reactions that produce optical emission in the FPD have not been firmly established, and that little information exists regarding the various emissive and non-emissive reaction pathways that consume analytes in flames [40]. In this context, another possibly relevant fact needs to be mentioned. Recently the photon yields (photons emitted per analyte atom) of several benchmark elements have been measured in a conventional FPD at optimized conditions. While these photon yields are some of the highest among the few ever established in chemiluminescent processes, on an absolute scale they are low. For example, the photon yields for sulfur (S_2^*), phosphorus (HPO^*) and iron (Fe^*) are 2×10^{-3}, 3×10^{-3} and 4×10^{-5}, respectively [41]. This may raise the theoretical question of whether the flame could induce larger amounts of analyte atoms to emit. Thus, for example, the question of response linearity might be connected to the apparent limits on photon yields.

However, if these yields are limited by reactions that concern primarily the analyte atom (e.g. if few emission precursors are formed) whereas the relevant energy carriers are abundant flame species (e.g. $H^\bullet$) then pseudo-first-order should prevail even in the very small flame of a ccFPD. In this case it can be argued that only a very small fraction of the analyte is involved in the process, further increasing the vast molar discrepancy between active flame and active analyte species. Ultimately though, as long as the complete decomposition/excitation/emission process of the analyte remains in doubt, so will the question of pseudo-first-order linearity, even with photon yields known.

Still, in the conventional FPD, linearity of the calibration curve is the typical case (although slight non-linearities can be encountered when conditions are not optimized). Furthermore, only one-order of magnitude of flow separates the small ccFPD flame from the conventional FPD flame. Finally, the calibration curves do not explicitly show the type of curvatures one would expect for cases in which a pseudo-first-order behavior changes into a second-order one. Given these facts, we again tend to believe that flame size per se is an unlikely reason for the calibration non-linearity and other response peculiarities occasionally observed in the ccFPD flame.

4. Conclusions

A novel, counter-current flame photometric detector with an “upside-down” flame has been designed and tested for future analytical use. The ccFPD exhibits exceptional flame stability over a very large range of gas flows. A number of standard compounds containing photometrically active elements such as sulfur, phosphorus, iron, ruthenium, lead, and manganese were examined. The results indicate that the ccFPD is capable of achieving minimum detectable limits similar to those of a conventional FPD, and that its S/N response increases dramatically for certain metals as the flame size decreases. While this is mostly attributable to a decrease in noise, a corresponding increase in analyte signal as the flame approaches its smallest size was also observed. These results, coupled with excellent simultaneous FID sensitivity (ionization response to carbon) indicate that useful analytical responses can be obtained from a counter-current flame and suggest that these might find applications in other analytical systems, particularly when very small or very large flows are to be accommodated, or when two-dimensional responses need to be obtained.

Acknowledgements

The authors are grateful to the Natural Sciences and Engineering Research Council of Canada for an operating grant in support of this research.

References

[1] G.A. Eiceman, H.H. Hill, J. Gardea-Torresdey, Anal. Chem. 70 (1998) 321.
[2] G.A. Eiceman, H.H. Hill, J. Gardea-Torresdey, Anal. Chem. 68 (1996) 291.
[3] G.A. Eiceman, H.H. Hill, J. Gardea-Torresdey, Anal. Chem. 72 (2000) 137.
[4] C.H. Wang, S.S. Lin, W.U. Hwang, H.S. Weng, Ind. Eng. Chem. Res. 41 (2002) 666.
[5] A. Macone, M. Nardini, A. Antonucci, A. Maggio, R.M. Matarese, J. Agric. Food Chem. 50 (2002) 2169.
[6] S. Otsuki, T. Nonaka, N. Takashima, W. Qian, A. Ishihara, T. Imai, T. Kabe, Energy Fuels 14 (2000) 1232.

[7] E. Mochizuki, T. Yamamoto, Y. Komiyama, H. Nakazawa, J. Agric. Food Chem. 46 (1998) 5170.
[8] T. Otake, J. Yoshinaga, Y. Yanagisawa, Environ. Sci. Technol. 35 (2001) 3099.
[9] J. Gui-bin, Z. Qun-fang, H. Bin, Environ. Sci. Technol. 34 (2000) 2697.
[10] P.L. Patterson, R.L. Howe, A. Abu-Shumays, Anal. Chem. 50 (1978) 339.
[11] S. Cheskis, E. Atar, A. Amirav, Anal. Chem. 65 (1993) 539.
[12] H. Jing, A. Amirav, J. Chromatogr. A 805 (1998) 177.
[13] N. Tzanani, A. Amirav, Anal. Chem. 67 (1995) 167.
[14] K.B. Thurbide, W.A. Aue, J. Chromatogr. A 684 (1994) 259.
[15] N.B. Lowery, W.A. Aue, J. Chromatogr. A 806 (1998) 305.
[16] X.-Y. Sun, W.A. Aue, J. Chromatogr. 467 (1989) 75.
[17] C. Shi, M.Sc. Thesis, Dalhousie University, Halifax, Nova Scotia, 1997.
[18] M. Dressler, Selective Gas Chromatographic Detectors, vol. 36 (Journal of Chromatography Library), Elsevier, Amsterdam, 1986, p. 133.
[19] R.S. Hutte, J.D. Ray, in: H.H. Hill, D.G. McMinn (Eds.), Detectors for Capillary Chromatography, Wiley, New York, 1992.
[20] P.J. Padley, T.M. Sugden, Proc. R. Soc. A 248 (1958) 248.
[21] R.S. Hobbs, G.F. Kirkbright, M. Sargent, T.S. West, Talanta 15 (1968) 997.
[22] K.M. Aldous, R.F. Browner, R.M. Dagnall, T.S. West, Anal. Chem. 42 (1970) 939.
[23] K.B. Thurbide, W.A. Aue, J. Chromatogr. A 905 (2001) 241.
[24] A.G. Gaydon, H.G. Wolfhard, Flames: Their Structure, Radiation, Temperature, third revised ed., Chapman & Hall, London, 1970.
[25] R.D. Lockett, B. Boulanger, S.C. Harding, D.A. Greenhalgh, Comb. Flame 119 (1999) 109.
[26] D.G. Vlachos, L.D. Schmidt, R. Aris, Comb. Flame 95 (1993) 313.
[27] K.B. Thurbide, C.D. Anderson, Analyst 128 (2003) 616.
[28] K.B. Thurbide, T.C. Hayward, Anal. Chim. Acta, submitted for publication.
[29] S. Zimmerman, J. Müller, Microsyst. Technol. 6 (2000) 241.
[30] S. Zimmerman, W. Wischhusen, J. Müller, Sens. Actuators B 63 (2000) 159.
[31] W.A. Aue, H. Singh, X.-Y. Sun, J. Chromatogr. A 687 (1994) 283.
[32] A.T. Blades, J. Chromatogr. Sci. 22 (1984) 120.
[33] R.S. Braman, Anal. Chem. 38 (1966) 734.
[34] G. Castello, G. D'Amato, M. Nicchia, J. Chromatogr. 521 (1990) 99.
[35] S.S. Brody, J.E. Chaney, J. Gas Chromatogr. 4 (1966) 42.
[36] W.E. Rupprecht, T.R. Phillips, Anal. Chim. Acta 47 (1969) 439.
[37] Y.-Z. Tang, Ph.D. Thesis, Dalhousie University, Halifax, Nova Scotia, 1987.
[38] W.A. Aue, X.-Y. Sun, J. Chromatogr. 633 (1993) 151.
[39] X.-Y. Sun, B. Millier, W.A. Aue, Can. J. Chem. 70 (1992) 1129.
[40] S.O. Farwell, C.J. Barinaga, J. Chromatogr. Sci. 24 (1986) 483.
[41] W.A. Aue, H. Singh, Spectrochim. Acta B 56 (2001) 517.